Spatiotemporal brain dynamics during recognition of the music of Johann Sebastian Bach

Bonetti L.[1,2*], Brattico, E. [1,6], Carlomagno, F. [1], Cabral J. [1,2,5], Stevner A. [1,2], Deco G.[4], Whybrow, P.C. [7], Pearce, M.[1], Pantazis, D.[8], Vuust P. [1] & Kringelbach M.L[1,2,3]

[1] *Center for Music in the Brain, Department of Clinical Medicine, Aarhus University & The Royal Academy of Music Aarhus/Aalborg, Denmark*

[2] *Centre for Eudaimonia and Human Flourishing, University of Oxford, UK*

[3] *Department of Psychiatry, University of Oxford, Oxford, United Kingdom*

[4] *Computational and Theoretical Neuroscience Group, Center for Brain and Cognition, Universitat Pompeu Fabra, Barcelona, Spain*

[5] *Life and Health Sciences Research Institute (ICVS), School of Medicine, University of Minho, 4710-057 Braga, Portugal*

[6] *Department of Education, Psychology, Communication, University of Bari Aldo Moro, Italy*

[7] *Semel Institute for Neuroscience and Human Behavior, University of California, Los Angeles, LA, USA*

[8] *McGovern Institute for Brain Research, Massachusetts Institute of Technology (MIT), Cambridge, USA*

**Corresponding author*

ABSTRACT

Music is a universal non-verbal human language, built on logical structures and articulated in balanced hierarchies between sounds, offering excellent opportunities to explore how the brain creates meaning for complex spatiotemporal auditory patterns. Using the high temporal resolution of magnetoencephalography in 70 participants, we investigated their unfolding brain dynamics during the recognition of Johann Sebastian Bach's original musical patterns compared to new variations thereof. Remarkably, the recognition of Bach's original music ignited a widespread music processing brain network comprising primary auditory cortex, superior temporal gyrus, insula, frontal operculum, cingulate gyrus, orbitofrontal cortex, basal ganglia and hippocampus. Furthermore, both activity and connectivity increased over time, following the evolution and unfolding of Bach's original patterns. This study shed new light on brain activity and connectivity dynamics underlying auditory patterns recognition, highlighting the crucial role of fast neural phase synchronization underlying meaningful, complex cognitive processes.

Introduction

Higher human brain function crucially depends on advanced pattern recognition and prediction of complex information [1,2]. This fast, seemingly effortless processing of information available in the present moment and its relation to the past and future is anything but effortless [3,4]. It depends on a complex chain of events, including stimulus identification, extraction of meaningful features, comparison with memory representation and prediction of upcoming stimuli [5,6].

For instance, a sequence of images, sounds, or words can be stored at several levels of detail, from specific items and their timing to abstract structure. Then, revisiting successfully the neural pathways formed during the encoding phase is crucial to properly predict and recognise the information conveyed by the constantly incoming external stimuli [7]. Neuroscientific research has widely investigated this central topic, focusing especially on processing and recognition of images and words [8,9]. Additionally, in the auditory domain, patterns have been extensively studied in the context of prediction error and automatic detection of environmental irregularities, as indexed by event-related components such as N100 and mismatch negativity (MMN) [10,11]. Indeed, this literature has highlighted that the brain is remarkably capable of recognising patterns and detecting deviations; key capacities to accomplish any complex cognitive function.

However, even if the interest for pattern recognition has increased across scientific fields and neuroscience, the brain mechanisms responsible for recognition of patterns acquiring meaning over time are not yet fully understood. Indeed, a recent paper by Stanislas Dehaene and colleagues [12] explicitly pointed out that future neuroscientific studies are called for to reveal the role of different brain areas in extracting and retrieving temporal sequences.

Thus, in this study, we focused on music, the human art that mainly acquires meaning through the combination of its constituent elements extended over time [13,14]. Indeed, beyond the strong emotional content evoked, music contains complex logical structures, articulated in carefully balanced hierarchies between sounds [14,15], yielding to meaningful messages and information that can be processed and recognised. Therefore, music is a great tool for investigating higher human brain processes implicated in the recognition of patterns unfolding over time.

In this regard, throughout music history, a unique place has been occupied by Johann Sebastian Bach's compositions that have stood the test of time. Bach's contrapuntal patterns, said to represent an ideal combination of refined logical structures and deeply emotional

melodies [16], have been crystallised into generations of minds, emerging as some of the most iconic and memorable artworks in human history.

Indeed, the interest for Bach's work has transcended the musical domain and inspired scientists. A famous example is represented by the acclaimed book entitled *Gödel, Escher, Bach: An Eternal Golden Braid* by Douglas Hofstadter [17]. This work highlighted similarities, common patterns and logical schemas of the outstanding creations of the composer J.S. Bach, the mathematician K. Gödel, and the artist M.C. Escher. While the necessary tools for studying brain responses were not available at the time, Hofstadter was very interested in discovering the commonalities that allow the brain to be able to understand the shared logical schemas and patterns, which ultimately makes music, arts and mathematics meaningful. Nowadays, with the advent of high temporal resolution whole-brain neuroimaging, we are finally in a position to study the music composed by Bach as a way to better understand the spatiotemporal dynamics of higher brain functions.

Here we thus used state-of-the-art neuroscientific techniques to study the brain activity elicited by musical sequences from the prelude in C minor BWV 847 by J.S. Bach and compared this to the response to musical variations, which were carefully matched to the original sequences in terms of information content and entropy. This allowed us to reveal the fundamental brain mechanisms underlying the recognition of musical patterns evolving over time.

Results

Experimental design and data analysis overview

In this study, we wanted to characterise the fine-grained spatiotemporal dynamics of the brain activity and connectivity during recognition of the musical patterns by Johann Sebastian Bach. During a session of magnetoencephalography (MEG), 70 participants listened to a musical instrumental digital interface (MIDI) version of the full prelude in C minor BWV 847 composed by Bach. As described in the Methods and depicted in **Figure 1A**, participants were then presented with short musical melodies corresponding to original excerpts of the Bach's prelude and carefully matched variations (in terms of information content and entropy, see Methods). Participants were asked to indicate whether each musical excerpt was an original Bach's pattern or a variation.

The analysis pipeline used in this study is illustrated in **Figure 1B** (and described in details in the Methods). This focused on extracting results using four main measures of brain activity: 1) sensor space, 2) beamformed source localised activity, 3) static source localised connectivity and 4) dynamic source localised connectivity.

First, we used multivariate pattern analysis and Monte Carlo simulations (MCS) on univariate tests of MEG sensor data. Second, we were interested in finding the brain sources of the observed differences and therefore we reconstructed the sources of the signal using a beamforming algorithm (**Figure 1C**) to track the brain activity related to each tone of the musical sequences (**Figure 1D**). Third, complementing our brain activity results, we computed the functional connectivity between different brain regions. We computed the static functional connectivity by computing Pearson's correlation between the envelopes of each pair of brain areas. Fourth, we investigated the functional connectivity dynamics.

Figure 2A depicts the Hilbert transform used to estimate the instantaneous phase synchronization between brain areas, while **Figure 2B** and **2C** illustrate the instantaneous functional connectivity matrices showing the connectivity patterns characterizing the brain at each time point. Similar to our analysis of brain activity, we analysed the brain connectivity patterns related to each tone of the musical sequences, as shown in **Figure 2D**. Here, we assessed both whole brain connectivity and degree centrality of brain regions.

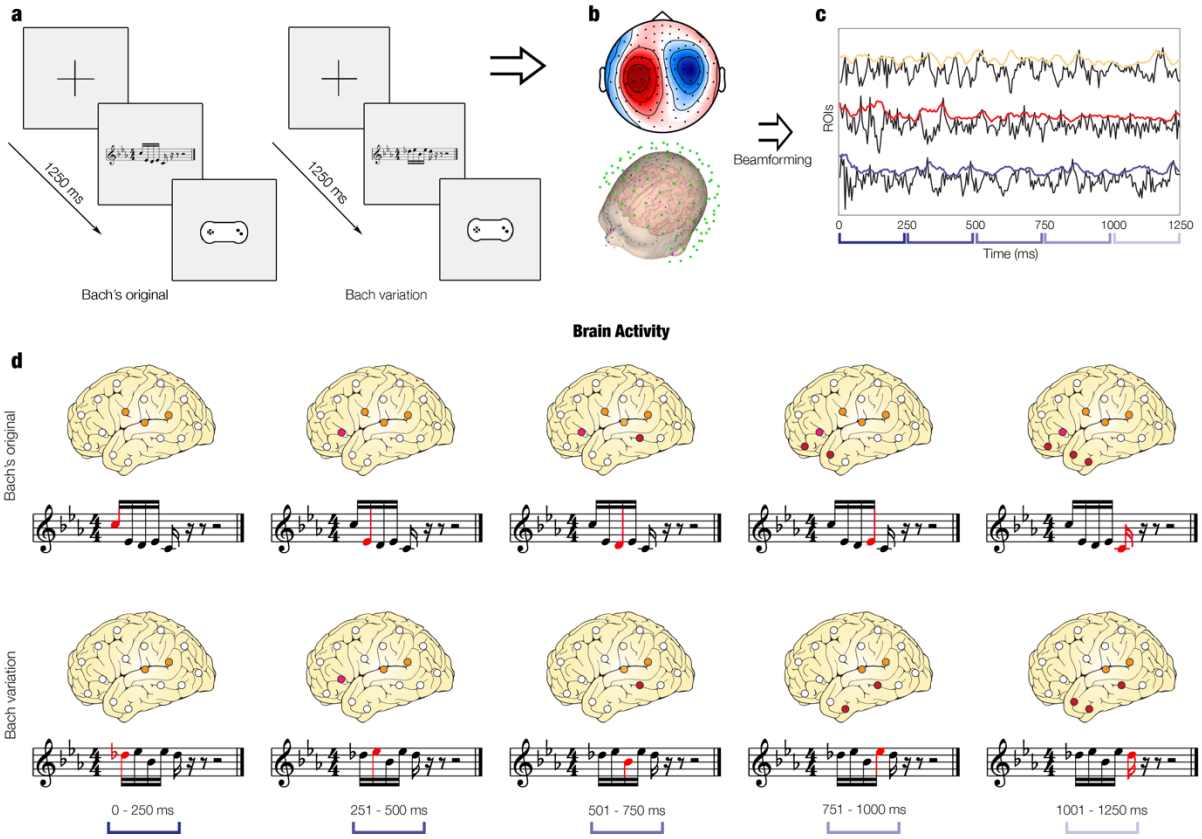

Figure 1. Experimental design and analysis methods.

a - *Graphical schema of the old/new paradigm. The paradigm consisted of presenting one excerpt at a time that could be a Bach's original pattern taken from the whole Bach's prelude that participants previously listened to (old) or a Bach variation pattern (new). In this figure, we depicted at first an example of Bach's original ('old') pattern (left, 2nd square) with the relative response pad that participants used to state whether they recognised the excerpt as 'old' or 'new' (left, 3th square). Then, we depicted an example of Bach variation ('new') pattern (right). The total number of trials was 80 (40 Bach's original and 40 Bach variation) and their order was randomized.* ***b*** *– We collected, pre-processed and analysed MEG sensor data by employing multivariate pattern analysis and MCS on univariate tests.* ***c*** *– We beamformed MEG sensor data into source space, providing time-series of activity originating from brain locations.* ***d*** *– We studied the source brain activity underlying the processing of each tone of the musical sequences for both experimental conditions.*

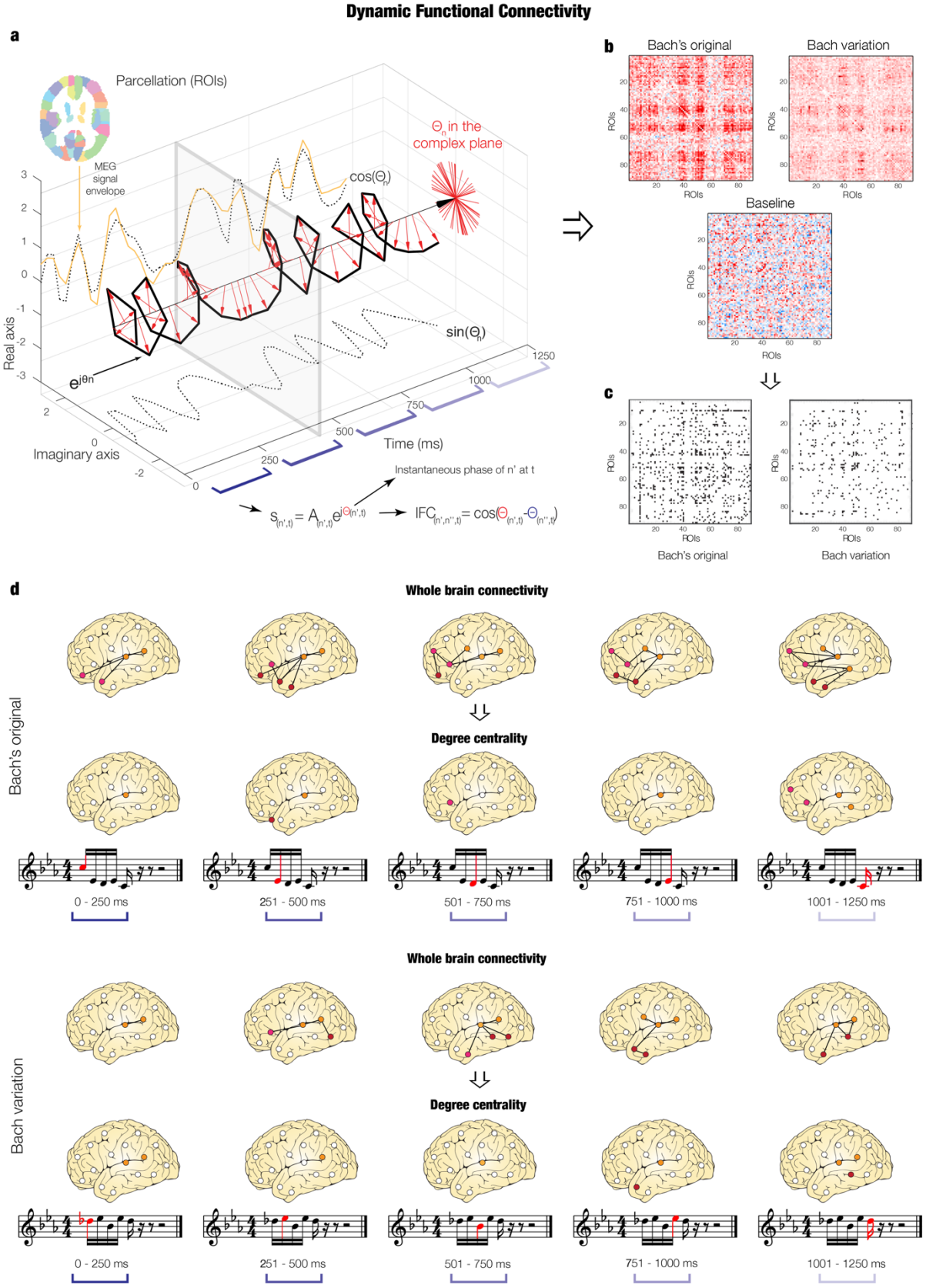

Figure 2. Overview of the analysis pipeline. a - *We computed the Hilbert transform of the envelope of each AAL parcellation ROI and estimated the phase synchronization by calculating the cosine similarity between the instantaneous phases of each pair of ROIs.* ***b*** *– We obtained for each time-point two IFC matrices for the task:*

one for Bach's original and one for Bach variation, plus an additional one for resting state that was used as baseline in the following steps. ***c*** *– We contrasted the task matrices vs the average of the baseline matrix to isolate the brain activity specifically related to the pattern recognition brain processes.* ***d*** *– We investigated the brain connectivity for each tone forming the musical sequences. First, we showed an illustration of the whole brain connectivity dynamics. Then, we depicted the significantly central ROIs within the whole brain network, estimated by applying MCS on the ROIs degree centrality calculated for each tone composing the musical sequences.*

MEG sensor data

Our first analysis was conducted on MEG sensor data and focused on the brain activity underlying the recognition of Bach's original musical patterns and variations. Specifically, we prepared 80 homo-rhythmic musical fragments lasting 1250 ms each (40 Bach's original and 40 Bach variations). On average participants correctly identified the 78.15 ± 13.56 % of the Bach's original excerpts (mean reaction times (RT): 1871 ± 209 ms) and the 81.43 ± 14.12 % of the Bach variations (mean RT: 1915 ± 135 ms). Successive MEG sensor data analysis was conducted on correct trials only.

Multivariate pattern analysis

As depicted in **Figure 3A**, we conducted a multivariate pattern analysis using a support vector machine (SVM) classifier (see details in the Methods section) to decode different neural activity associated with the recognition of Bach's original and variation. This analysis resulted in a decoding time-series showing how neural activity differentiated the two experimental conditions. The decoding time-series was significantly different from chance level in the time range 0.8 - 2.1 seconds from the onset of the first tone ($p < .026$, false-discovery rate (FDR)-corrected, **Figure 3A**, top left).

To evaluate the persistence of discriminable information over time, we applied a temporal generalisation approach by training the SVM classifier at a given time point t, as before, but testing across all other time points. Intuitively, if representations are stable over time, the classifier should successfully discriminate signals not only at the trained time t, but also over extended periods of time that share the same neural representation. FDR-corrected ($p < .005$) results are depicted in **Figure 3A** (top right) showing that performance of the classifier was significantly above chance even a few hundreds of milliseconds beyond the diagonal.

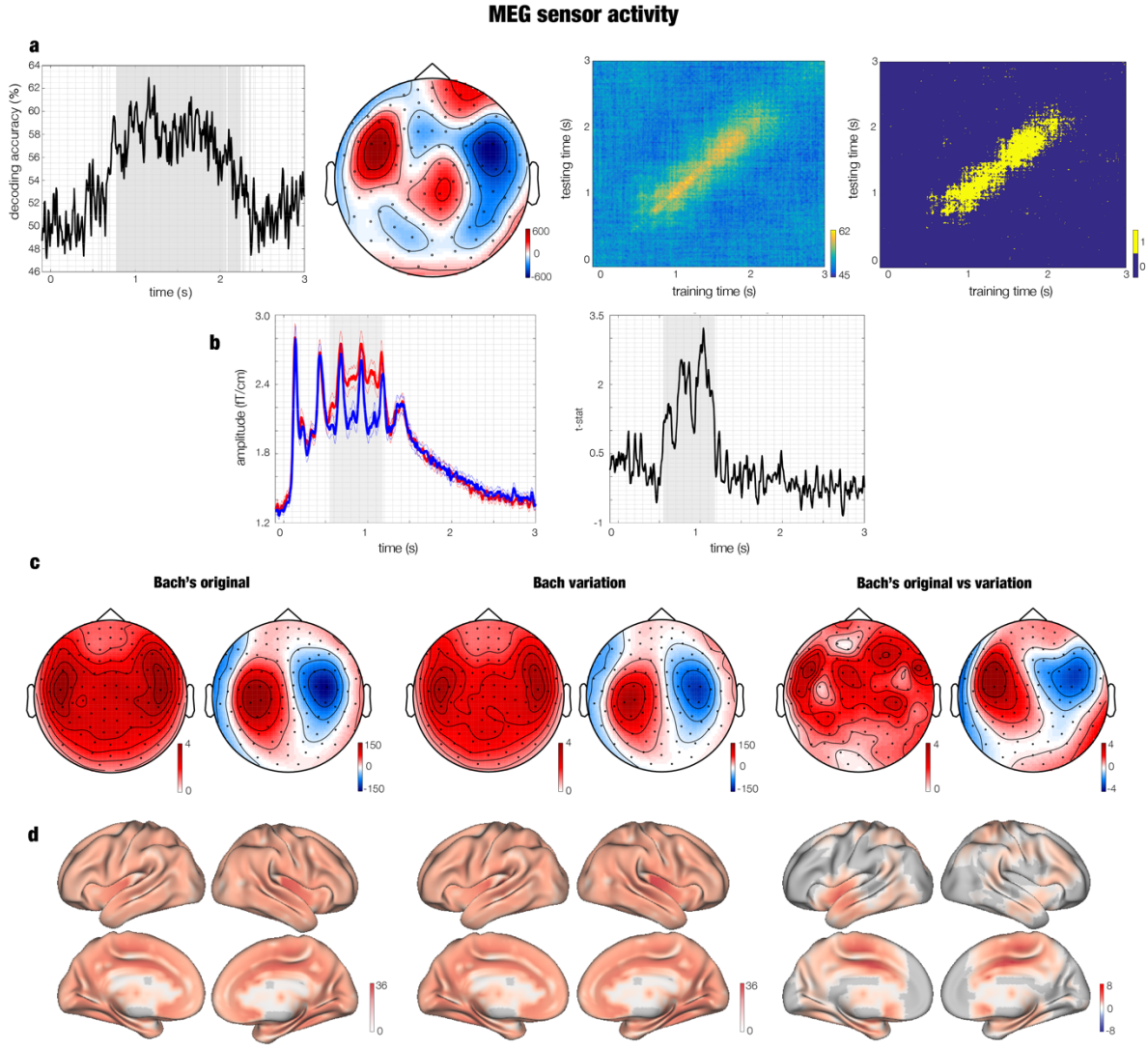

Figure 3. Bach's original vs variation neural activity: cluster I. a – *Multivariate pattern analysis decoding the different neural activity associated to Bach's original vs variation. Decoding time-series (left), spatial patterns depicted as topoplot (middle left), temporal generalization decoding accuracy (middle right) and statistical output of significant prediction of training time on testing time (right).* ***b –*** *The left plot shows the amplitude associated to Bach's original (red) and variation (blue). The right plot illustrates the t-statistics related to the contrast between Bach's original vs variation. Thinner lines depict standard errors. Both plots represent the average over the gradiometer channels forming the significant cluster outputted by MEG sensor MCS.* ***c –*** *Three couples of topoplots showing brain activity for gradiometers (left of each pair, fT/cm) and magnetometers (right of each pair, fT) within the significant time-window emerged from MCS. First couple of topoplots depicts Bach's original neural activity, second couple refers to Bach variation, while the third one represents the statistics (t-values) contrasting Bach's original vs variation brain activity.* ***d –*** *Neural sources of Bach's original (left), variation (middle) and their contrast (right). The values are t-statistics.*

Univariate tests and Monte Carlo simulations

The multivariate pattern analysis is a powerful tool that requires relatively few pre-processing steps for returning an estimation of neural activity that discriminates two or more experimental conditions. However, this technique does not provide directional information, that is, it does not identify which experimental condition yields a stronger neural signal. To answer this question, we performed independent univariate t-tests between conditions for each time-sample and each MEG channel and then corrected for multiple comparisons using a cluster-based Monte Carlo simulation (MCS) approach.

First, we contrasted Bach's original vs variation (t-test threshold = .01, MCS threshold = .001, 1000 permutations), considering the positive t-values only (which is when Bach's original was associated to a stronger brain activity than Bach variation). We performed this analysis in the time-range 0 – 2.5 seconds by using combined planar gradiometers only. This procedure yielded the identification of one main significant cluster, as depicted in **Figure 3B** and **3C** and reported in details in **Tables 1** and **ST2**. Then, on the basis of the significant cluster appearing, we computed the same algorithm one more time for magnetometers only, within the significant time-range emerged for the first MCS (0.547 – 1.180 seconds, $p < .001$). This two-step procedure was necessitated by the sign ambiguity typical of magnetometer data (see Methods for details).

Then, the same procedure was carried out by considering the results where the brain activity associated to Bach variation exceeded the one elicited by Bach's original phrase. This analysis returned eight small significant clusters (size range: 6 – 14, $p < .001$) shown in **Table ST1**.

Cluster number	**Size**	**Channels**	**Time-range (s)**	***p***
Gradiometers (Bach's original vs Bach variation)				
1	2117	90	0. 547 – 1.180	< .001
Magnetometers – positive (Bach's original vs Bach variation)				
1	817	24	0.627 – 1.180	< .001
Magnetometers – negative (Bach's original vs Bach variation)				
1	190	18	0.727 – 0.880	< .001
2	168	15	0.960 – 1.133	< .001

***Table 1**. Significant clusters of MEG sensors emerged from MCS contrasting Bach's original vs variation. The table depicts these clusters independently for gradiometers and positive and negative magnetometers.*

Source reconstructed data

To identify the neural sources of the signal, we employed a beamforming approach and computed a general linear model (GLM) for assessing, at each time-point, the independent neural activity associated to the two conditions as well as their contrasts.

Main cluster of Bach's original vs variation

We identified the neural sources of the gradiometer significant cluster emerging from the MEG sensor data when contrasting Bach's original vs variation. Here, we performed one permutation test in source space, with an α level of .05, which, in our case, corresponds to a cluster forming threshold of t = 1.7. As depicted in **Figure 3D**, results showed a strong activity originating in the primary auditory cortex, insula, hippocampus, frontal operculum, cingulate cortex and basal ganglia. Detailed statistics are provided in **Table ST3**.

Dynamic brain activity during development of musical patterns

Then, to reveal the specific brain activity dynamics underlying the recognition of the musical sequence, we carried out a further analysis for each musical tone forming the pattern. Here, we adopted a cluster forming threshold of t = 2.7 (see Methods for details). As depicted in **Figure 4A** and **4B**, we found significant activity within primary auditory cortex and insula, especially in the right hemisphere, for both experimental conditions. This activity decreased over time, following the unfolding of the musical sequences. Conversely, the contrast between Bach's original vs variation gave rise to a burst of activity for Bach's original increasing over time, especially with regards to the last three tones of the musical sequences, as shown in **Figure 4C**. This activity was mainly localised within hippocampus, frontal operculum, cingulate cortex, insula and basal ganglia. We report detailed clusters statistics in **Table ST4**.

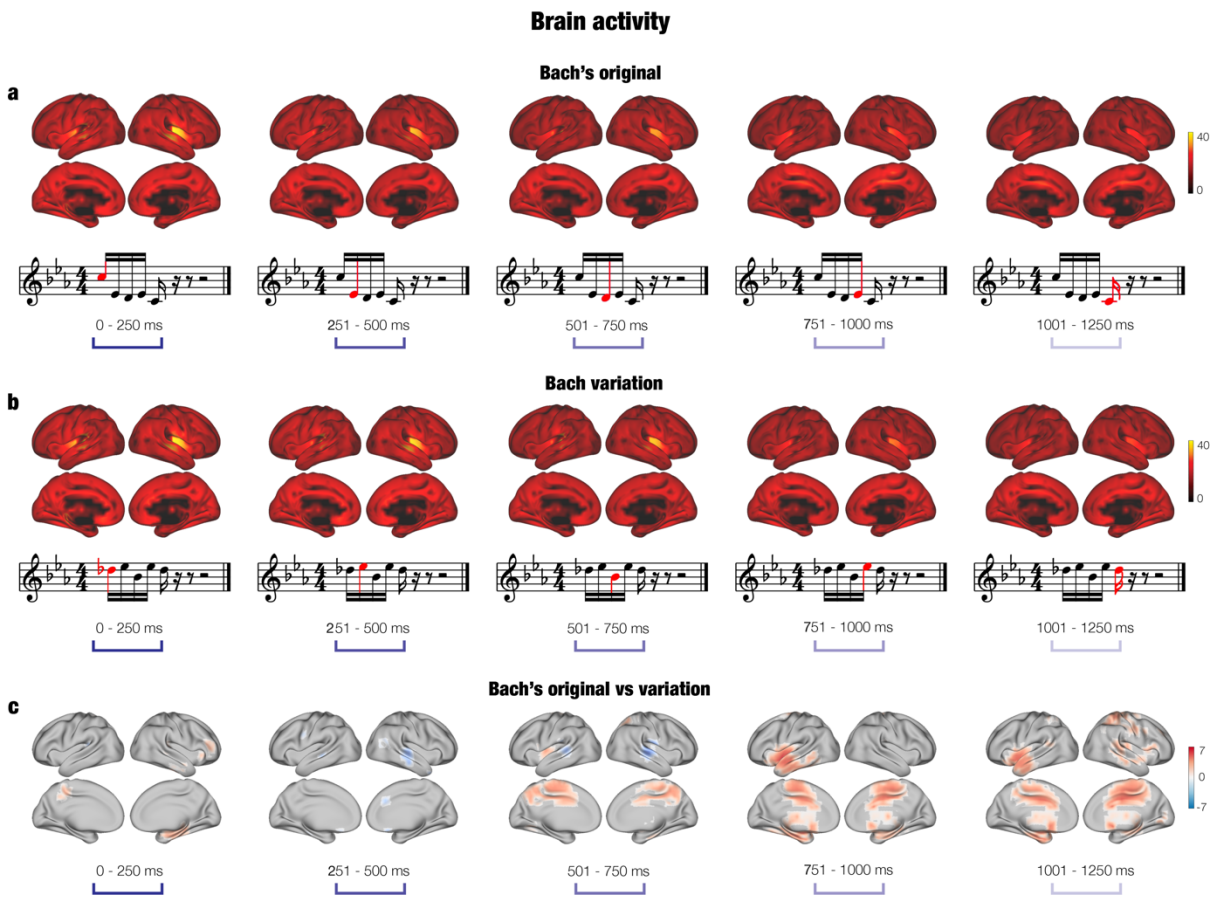

Figure 4. Brain activity over time. a *– Brain activity (localized with beamforming) associated to the recognition task for Bach's original (top row) and musical notation of one example trial for Bach's original pattern (bottom row). Red tones illustrate the dynamics of the musical excerpt.* ***b*** *– Brain activity concerning Bach variation (top row) and musical representation of one example trial for Bach variation (bottom row).* ***c*** *– Contrast (t-values) over time between brain activity associated to Bach's original vs Bach variation.*

Functional connectivity

In order to obtain a better understanding of the brain dynamics underlying recognition, we complemented our brain activity results with an investigation of the static and functional connectivity.

Static functional connectivity

MEG pre-processed data was constrained to the 90 non-cerebellar parcels of the automated anatomic labelling (AAL) parcellation and corrected for source leakage. First, we computed Pearson's correlations between the envelopes of the time-series of each pair of brain areas. This procedure was carried out for both task (in this case without distinguishing between Bach's original and variation) and resting state (used as baseline) for each participant and five frequency bands: delta, theta, alpha, beta and gamma. Then, we tested the overall connectivity strengths of the five frequency bands during auditory recognition by employing analysis of variance (ANOVA). The test was significant ($F(4,330) = 187.02$, $p < 1.0e\text{-}07$). As depicted in **Figure 5A** and **5B**, post-hoc analysis highlighted especially that theta band had a stronger connectivity profile than all other frequency bands ($p < 1.0e\text{-}07$).

To detect the significance of each brain region centrality within the whole brain network for the auditory recognition task, we contrasted the brain connectivity matrices associated to the task vs baseline by performing a Wilcoxon signed-rank test for each pair of brain areas. Then, the resulting z-values matrix was submitted to a degree MCS (see Methods for details). We computed this analysis independently for the five frequency bands and therefore we considered significant the brain regions whose p-value was lower than the α level divided by 5 (2.0e-04). The results for theta band are depicted in **Figure SF1** and reported as follows: left Rolandic operculum ($p < 1.0e\text{-}07$), insula ($p < 1.0e\text{-}07$), hippocampus ($p = 5.5e\text{-}05$), putamen ($p < 1.0e\text{-}07$), pallidum ($p < 1.0e\text{-}07$), caudate ($p = 1.1e\text{-}05$), thalamus ($p < 1.0e\text{-}07$), Heschl's gyrus ($p < 1.0e\text{-}07$), superior temporal gyrus ($p < 1.0e\text{-}07$), right superior temporal gyrus ($p = 1.1e\text{-}06$), Heschl's gyrus ($p < 1.0e\text{-}07$), thalamus ($p < 1.0e\text{-}07$), parahippocampal gyrus ($p = 4.3e\text{-}05$), pallidum ($p < 1.0e\text{-}07$), putamen ($p < 1.0e\text{-}07$), amygdala ($p < 1.0e\text{-}07$), insula ($p < 1.0e\text{-}07$) and Rolandic operculum ($p < 1.0e\text{-}07$). Additional results related to the other frequency bands are reported in Supplementary Materials (**SR1**).

Conversely, the degree MCS of the contrasts between Bach's original vs variation yielded no significant results.

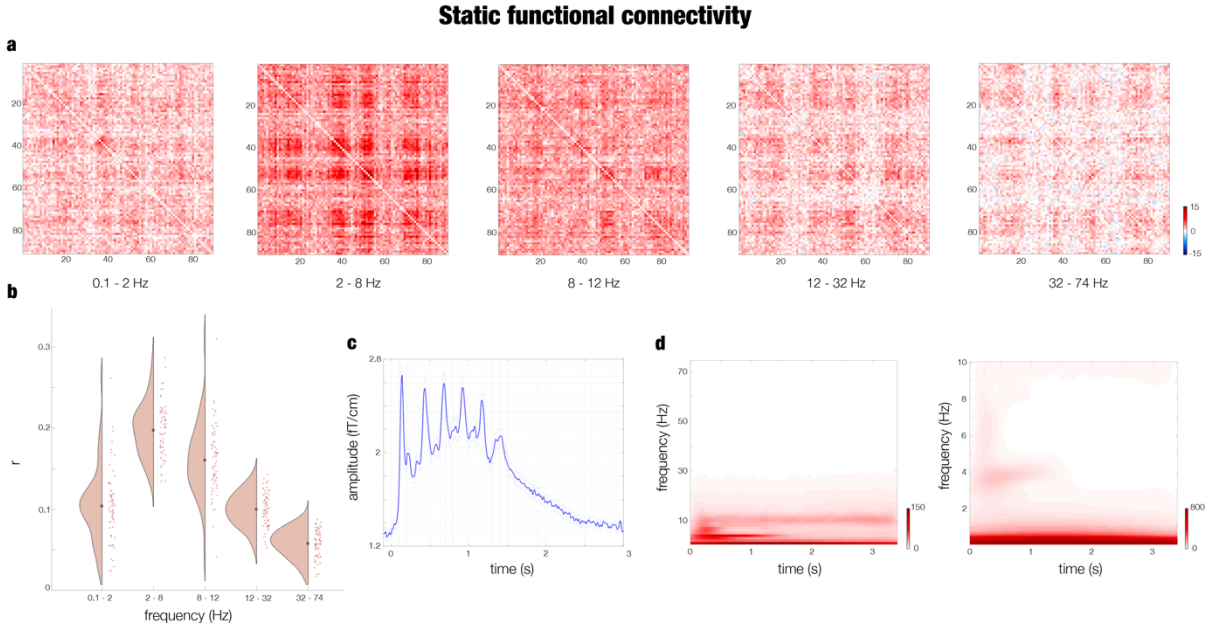

Figure 5. Static functional connectivity. ***a*** *– Contrast between recognition task (Bach's original and variation averaged together) and baseline SFC matrices calculated for five frequency bands: delta (0.1 – 2 Hz), theta (2 – 8 Hz), alpha (8 – 12 Hz), beta (12 – 32 Hz), gamma (32 – 74 Hz).* ***b*** *– Violin-scatter plot showing the average of the SFC matrices over their two dimensions for all participants.* ***c*** *– Averaged MEG gradiometer channels waveform of the brain activity associated to the recognition task.* ***d*** *– Power spectra for all MEG channels associated to the recognition task. The first power spectra matrix reflects the analysis from 1 to 74 Hz in 1-Hz intervals, while the second from 0.1 to 10 Hz in 0.1-Hz intervals.*

Dynamic functional connectivity

Expanding on the analysis of static functional connectivity, we focused on the brain connectivity patterns evolving dynamically over time. Thus, by employing Hilbert transform and cosine similarity, we computed the phase synchronization between each pair of brain areas, obtaining one instantaneous functional connectivity (IFC) matrix for each musical tone (see Methods for details). Then, we calculated the contrast between the IFC matrices associated to the two conditions vs the baseline (illustrated in the top rows of **Figure 6A** and **6B**, and in **Figure SF2**). Subsequently, as reported in the middle rows of **Figure 6A** and **6B**, we computed the significantly central brain regions within the whole brain network for each tone forming the musical pattern and both Bach's original and variation. We tested statistical significance by using MCS. Since we repeated this test 10 times (two conditions and five tones), we used a threshold = 1.0e-04, obtained dividing the α level (.001) by 10. Detailed

statistics are reported in **Table ST5**. Finally, as depicted in **Figure 6C** (top row), we contrasted the IFC matrices for Bach's original vs variation and then we estimated the correspondent significantly central brain regions (**Figure 6C**, bottom row). These results are reported in details in **Tables 2** (Bach's original) and **ST6** (Bach variation).

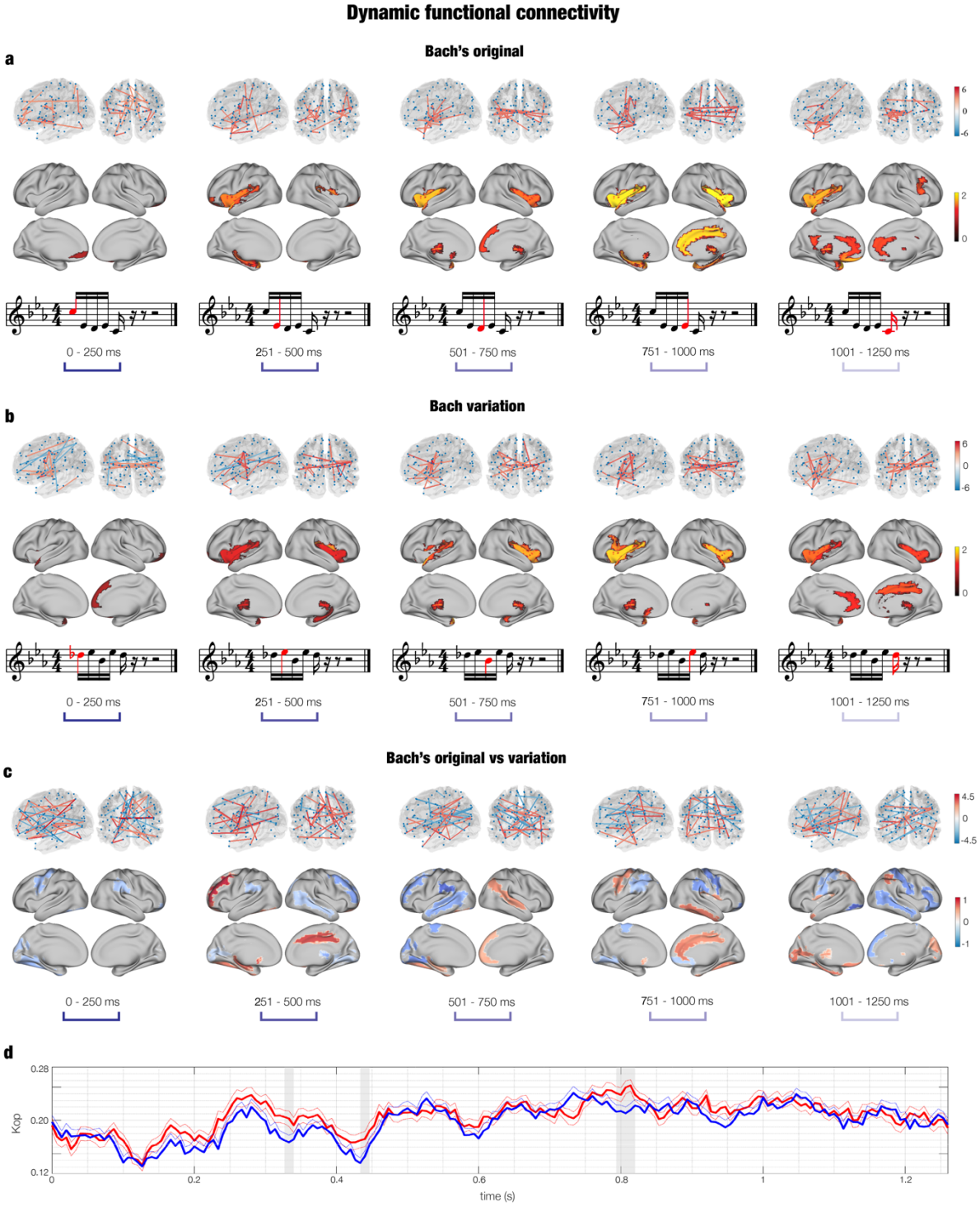

Figure 6. Dynamic functional connectivity. a *– DFC calculated for each tone composing Bach's original musical pattern. The top row depicts the whole brain connectivity in a brain template (each pair presents the left hemisphere and a posterior view of the brain). Values refers to Wilcoxon sign-rank test z-values computed for Bach's original vs baseline DFC matrices. The bottom row illustrates the significantly central ROIs within the whole brain network over time, as assessed by MCS. Values show the average z-value between the significant ROIs and the rest of the brain regions.* ***b*** *– DFC calculated for Bach variation. The depiction is analogous to the one described for point a).* ***c*** *– DFC computed by contrasting Bach's original vs variation. The*

depiction is analogous to the one described for point a). ***d*** *– Kuramoto order parameter calculated for each time-point for both Bach's original (red line) and variation (blue line). Grey areas show the significant time-windows emerged by MCS.*

Tone 1			
Left central ROIs	*p*	*Right central ROIs*	*p*
Tone 2			
Middle frontal orbital cortex	< 1.0e-07	Superior orbitofrontal cortex	< 1.0e-07
Hippocampus	< 1.0e-07	Middle cingulate gyrus	< 1.0e-07
Middle frontal gyrus	< 1.0e-07		
Caudate	< 1.0e-07		
Fusiform gyrus	8.8e-05		
Tone 3			
Fusiform gyrus	< 1.0e-07	Angular	< 1.0e-07
Hippocampus	2.2e-05	Superior temporal gyrus	< 1.0e-07
		Ventro-med prefrontal cortex	2.2e-05
		Fronto-superior medial cortex	1.0e-04
Tone 4			
Caudate	< 1.0e-07	Anterior cingulum gyrus	< 1.0e-07
Precentral gyrus	2.2e-05	Inferior temporal gyrus	< 1.0e-07
		Fusiform gyrus	1.1e-05
		Middle cingulum gyrus	6.6e-05
Tone 5			
Parahippocampal gyrus	< 1.0e-07	Parietal inferior lobule	< 1.0e-07
Fronto-medial orbital cortex	< 1.0e-07		
Calcarine	< 1.0e-07		
Parietal superior lobule	< 1.0e-07		
Thalamus	< 1.0e-07		
Temporal pole middle	< 1.0e-07		
Rolandic operculum	5.5e-05		

Table 2. *Significantly central ROIs for Bach's original vs variation contrast of DFC matrices. The calculation has been done independently for each tone forming the musical patterns.*

Kuramoto order parameter

Finally, to obtain a global measure of instantaneous connectivity within the brain over time, we computed the Kuramoto order parameter (see Methods) for the two experimental conditions and each time-point of the recognition task, obtaining two time-series. We contrasted them by performing t-tests and corrected for multiple comparisons through a 1-dimensional (1D) MCS. Results, depicted in **Figure 6D**, showed a significant difference for the following time-ranges: 0.793 – 0.820 seconds (p = 4.5e-05), 0.327 – 0.340 seconds (p = .01) and 0.433 – 0.447 seconds (p = .01). In all three cases, Bach's original was characterized by a significantly higher Kuramoto order parameter than Bach variation.

Discussion

In this study, we were able to detect the fine-grained spatiotemporal dynamics of the brain activity and connectivity during recognition of the musical patterns by Johann Sebastian Bach compared to carefully matched variations.

First, by using a multivariate pattern analysis and MCS of massive univariate data, we found that the brain activity elicited by Bach's original music compared to the variations gave rise to significant changes in widespread regions including primary auditory cortex, superior temporal gyrus, cingulate gyrus, hippocampus, basal ganglia, insula and frontal operculum.

Second, we investigated this important finding further by estimating static and dynamic functional brain connectivity evolving over time. Here, the recognition of the musical patterns was accompanied by significant centrality within the whole brain network of a number of brain regions including the insula, hippocampus, cingulate gyrus, auditory cortex, basal ganglia, frontal operculum, subgenual and orbitofrontal cortices. Notably, these connectivity patterns emerged more clearly for the last three tones of the five tones of the musical patterns and, even if similar across conditions, they were found to be stronger for Bach's original phrases than for the variations. This finding lends strong support to the intriguing proposal by Changeux that recognition of meaningful art has the ability to ignite large brain networks [18]. As such, our results also make a significant contribution to identifying the brain networks engaged in eudaimonia, the meaningful pleasure evoked by music [19].

Brain activity dynamics of auditory pattern recognition

The brain activity recorded during the recognition of the musical sequences was coherent with a large number of studies showing auditory processes associated to primary auditory cortex and insula [20,21]. Remarkably, contrasting Bach's original phrases versus variations, we observed stronger activity underlying the recognition of original patterns in brain areas related to memory recognition such as hippocampus, medial temporal cortices [22,23] and cingulate cortices [24]. Additionally, the recognition of Bach's original was associated to a stronger activity of brain regions previously related to evaluative processes [25,26] and pleasure [27,28] such as cingulate gyrus, subgenual cortices as well as parts of the basal ganglia. Finally, recognition of Bach's original was accompanied by stronger activity in brain

regions responsible for fine-grained auditory elaboration and prediction error such as the inferior temporal cortex [29] and insula [30,21].

Brain functional connectivity dynamics of auditory patterns recognition

In addition, to investigating the significant differences in brain activity ignited by Bach's original patterns compared to the variations, we conducted detailed functional connectivity analyses. Since music is a language that acquires meaning over time, we mainly focused on dynamic functional connectivity analyses to assess whether different connectivity patterns were associated to different parts of the musical sequence. Remarkably, our connectivity analysis revealed both important similarities and differences within the evolving brain activity over time.

A key relevant difference was that while the activity of the brain areas decreased over time, the degree centrality and connectivity between brain regions became clearer with the temporal development of the auditory patterns. Moreover, primary auditory cortex did not play a crucial role, while the main connectivity patterns emerged for brain regions related to higher sound and linguistic elaborations such as insula, inferior temporal cortex [30,29] and frontal operculum [31]. Furthermore, we also observed other central brain areas that have been previously related to evaluative processes such as orbitofrontal and subgenual cortices [32,25] and memory such as hippocampus [33] and basal ganglia [34]. Notably, the connectivity patterns and centrality of brain regions were stronger for Bach's original phrases than the variations. This evidence suggests the relevance of the synchronization between brain areas over their mere activation to understand the brain networks underlying complex memory processes.

Conversely, a crucial similarity between brain activity and connectivity analyses was that compared to the variations, the recognition of Bach's original patterns ignited the shared common music processing brain network in terms of both activity and connectivity. As mentioned earlier, Changeux [18] proposed that processing and recognition of certain privileged classes of stimuli including meaningful artistic works can ignite the brain areas forming the global workspace [18]. Authors defined the global workspace as a privileged network of brain areas, where conscious information is processed in terms of memory, attention and valence, and subsequently broadcast and made available to the whole brain [35,36,37]. As predicted by Changeux's hypothesis, the recognition of Bach's original patterns – over and above the variations – led to stronger ignition of putative regions in the

global workspace such as hippocampus, cingulate gyrus, orbitofrontal cortex and frontal operculum, perhaps reflecting the unique nature of that meaningful music.

A further central theory in the neuroscientific field that can be related to our results is predictive coding. In this framework, the brain is considered a generator of models of expectations of the incoming stimuli. Recently, this theory has been linked to complex cognitive processes, finding a remarkable example in the neuroscience of music [2]. In their work, Koelsch and colleagues suggested that the perception of music is the result of an active listening process where individuals constantly formulate hypothesis about the upcoming development of musical sentences, while those sentences are actually evolving and unfolding their ambiguities. Our study is consistent with this perspective, where the brain predicts the upcoming sounds of the musical patterns leading to at least two separable outcomes. On the one hand, there is activity in the primary auditory cortex, responsible for the first sensorial processing of tones, and decreasing over time. On the other hand, the ignition of brain areas related to memory and evaluative processes is increasing over time and stronger for Bach's original phrases than for the variations. Indeed, this would suggest that the brain has formulated predictions of the upcoming sounds on the basis of the memory trace previously stored during the encoding part of our experimental task. The match between those predictions and the actual sounds presented to participants may lead to the ignition of the brain areas that we observed in our experiment.

In line with the predictive coding framework, our results expanded also the neuroscientific literature on prediction error. Indeed, previous research using paradigms that required active encoding and evaluation of the stimuli to formulate predictions and drive decision-making processes has highlighted a prominent role of the anterior cingulate gyrus [37,38] and a relevant contribution of hippocampal areas [39,40]. Furthermore, in the auditory domain, traditionally prediction error has been investigated through the brain response to violations of auditory regularity, as indexed by event-related components such as N100 and MMN [41,10]. Additionally, more recent research has shown a hierarchical organization of prediction error processes occurring within the auditory cortex [42,43]. However, the majority of these auditory studies employed varied versions of the oddball paradigm or more complex tasks that did not require conscious elaboration of the stimuli, making it difficult to interpret the results in terms of higher brain functioning.

In contrast, in the current study we utilised an auditory paradigm that required participants to make active choices on the basis of prediction processes. Indeed, in line with the previous literature, we detected a prominent role played by cingulate cortex, hippocampus and

auditory cortex to establish whether a musical excerpt was a Bach's original or a variation. Notably, we observed hippocampus and cingulate gyrus to be central within the whole brain network when the incoming stimuli matched the prediction made by the brain (e.g. when listening to Bach's original), while the auditory cortex appeared more central for signalling a violation within the musical sequence expectation (e.g. when listening to Bach variation).

Static functional connectivity and event-related fields

Additionally, to increase the reliability of our findings, we complemented our main results on spatiotemporal dynamics of brain activity and connectivity with more traditional approaches such as static functional connectivity and analysis of MEG sensors.

For the static functional connectivity, we computed Pearson's correlations between the envelopes of each pair of brain areas and then studied the centrality of brain regions within whole-brain networks. We detected the most prominent connectivity patterns associated to music recognition for theta band (2 – 8 Hz), highlighting a large network of brain regions including primary auditory cortex, superior temporal gyrus, frontal operculum, insula, hippocampus and basal ganglia. As expected, the static functional connectivity network was very similar to the dynamic functional connectivity ones and involved brain regions previously related to auditory [44], memory [22,23] and evaluative processes [26].

Importantly, the static functional connectivity analysis failed to detect differences between Bach's original phrases and variations. This shows that to capture the fine-grained brain functioning underlying recognition of original musical patterns, it was crucial to employ methods designed to detect the dynamic unfolding of the brain connectivity.

We also investigated our data by focusing on MEG sensor analysis. In this regard, we found that brain activity was reflected by two event-related fields (ERF) components: N100 to each sound and a slow negativity following the entire duration of the musical patterns.

While the N100 associated to each tone represented a well-known finding, to the best of our knowledge the detection of the slow negative component associated to pattern recognition has never been described earlier. Indeed, even if this negative waveform shared similarities with well-established ERF components such as contingent negative variation (CNV) [45], P300 and P600 [46], previous literature has never associated an auditory recognition task to a slow negative component such as the one that we described. Thus, our results provided new insights and may contribute to develop future perspectives also within the framework of ERF and MEG sensor analysis.

Conclusion

In conclusion, our findings have identified the spatiotemporal unfolding of brain activity elicited by the recognition of the music of J.S. Bach compared to carefully matched variations thereof. These results reveal the brain networks involved in recognising music that many describe as eliciting deeply meaningful musical experiences – similar to those proposed in the 'Gödel, Escher and Bach' book mentioned in the introduction [17].

As an aside, an anecdote from Bach's contemporary Christian Schubart reminds us of the importance of creating real, lasting art – rather than mere variations - was never far from Bach's mind. Bach's son Johann Christian Bach recounted playing around with a variation of Bach's musical compositions which woke up Bach, prompting him to get up, reprimand his son and play the correct ending.

More research is needed to reveal what it is about Bach's music that so speaks to both the mind and emotion not just when already familiar but even when it is first encountered. Still, the present results reveal some of the brain mechanisms underlying Hofstadter's seminal ideas on what makes us recognise art as meaningful. In line with the proposal by Changeux [18], our results show that recognising Bach's music - which is generally considered a high point of Western musical art – ignites widespread brain networks that may contribute to feeling of deeply meaningful music, and perhaps even the elusive state of eudaimonia. Indeed, our results using state-of-the-art neuroimaging and analysis methods highlight how the integration of brain activity and fast-scale phase synchronization analyses, combined with Bach's high meaningful musical patterns, provide a unique opportunity to understand the brain functioning underlying complex cognitive processes - and can perhaps even shed light on how art becomes meaningful for the brain.

Methods

Participants

The study comprised 70 volunteers, composed by 36 males and 34 females (age range: 18 – 42 years old, mean age: 25.06 ± 4.11 years). Since our experiment involved a musical piece usually played by classical pianists, we recruited 23 classical pianists (13 males and 10 females, age range: 18 – 34 years old, mean age: 24.83 ± 4.10 years old), 24 non-pianist musicians (12 males and 12 females, age range: 19 - 42 years old, mean age: 24.54 ± 4.75), and 23 non-musicians (11 males and 12 females, age range: 21 – 35 years old; mean age: 25.86 ± 3.34). The sample regarding functional connectivity analysis slightly differed (three participants had to be discarded due to technical problems during acquisition) consisting of 67 participants (34 males and 33 females, age range: 18 – 42 years old, mean age: 25.00 ± 4.18 years). Specifically, 21 were non-pianist musicians (10 males and 11 females, age range: 42 – 19 years old, mean age: 24.29 ± 5.02 years), 23 classical pianists (13 males and 10 females, age range: 18 – 34 years old, mean age: 24.83 ± 4.10 years) and 23 non-musicians (11 males and 12 females, age range: 21 – 35 years old; mean age: 25.86 ± 3.34 years).

All the experimental procedures were carried out complying with the Declaration of Helsinki – Ethical Principles for Medical Research and were approved by the Ethics Committee of the Central Denmark Region (De Videnskabsetiske Komitéer for Region Midtjylland) (Ref 1-10-72-411-17).

Experimental design and stimuli

To study the brain dynamics of musical pattern recognition, we employed an old/new [47] auditory pattern recognition task during MEG recording. First, participants were requested to listen to four repetitions of a MIDI homo-rhythmic version of the right-hand part of the entire prelude in C minor BWV 847 composed by J.S. Bach (total duration of about 10 minutes). Second, they were presented with 80 short musical excerpts lasting 1250 ms each and requested to indicate whether each excerpt belonged to the prelude by Bach (Bach's original, old) or was a variation of the original patterns (Bach variation, new). A graphical depiction of the experimental design is reported in **Figure 1A.** Successive analyses were performed on correctly recognised trials only. Both the entire prelude and the excerpts were created by using Finale (MakeMusic, Boulder, CO) and then presented by adopting Presentation software (Neurobehavioural Systems, Berkeley, CA).

Notably, to extract the original Bach's excerpt and to create their variations, we matched the average information content (IC) and entropy (H) estimated for each tone of the original excerpts (mean IC: 5.70 ± 1.73, mean H: 4.70 ± .33) and the variations (mean IC: 5.92 ± 1.81, mean H: 4.78 ± .35) by using Information Dynamics of Music (IDyOM) [48]. This method uses machine learning to return a value of IC for the target note on the basis of a combination of the preceding notes and of a set of rules learned from a large set of prototypical pieces of Western music. Formally, the IC represents the minimum number of bits required to encode e_i and is described by the equation (1):

$$IC\left(e_i|e_{(i-n)+1}^{i-1}\right) = \log_2 \frac{1}{p(e_i|e_{(i-n)+1}^{i-1})} \tag{1}$$

Where $p(e_i|e_{(i-n)+1}^{i-1})$ is the probability of the event e_i given a previous set of $e_{(i-n)+1}^{i-1}$ events.

The entropy gives a measure of the certainty/uncertainty of the upcoming event given the previous set of $e_{(i-n)+1}^{i-1}$ events and is calculated by the equation (2):

$$H\left(e_{(i-n)+1}^{i-1}\right) = \sum_{e \in A} p(e_i|e_{(i-n)+1}^{i-1}) IC(e_i|e_{(i-n)+1}^{i-1}) \tag{2}$$

Equation (2) shows that if the probability of a given event e_i is 1, the probability of the other events in A will be 0 and therefore H will be equal to 0 (maximum certainty). On the contrary, if all the events are equally likely, H will be maximum (maximum uncertainty). Therefore, IDyOM returns an estimation of the predictability of each tone and uncertainty with which it can be predicted, coherently with the human perception [49].

In the same or another day than the MEG recording, we collected structural images for each participant by employing magnetic resonance imaging (MRI).

Data acquisition

We acquired both MRI and MEG data in two independent sessions. The MEG data was acquired by employing an Elekta Neuromag TRIUX system (Elekta Neuromag, Helsinki, Finland) equipped with 306 channels. The machine was positioned in a magnetically shielded room at Aarhus University Hospital, Denmark. Data was recorded at a sampling rate of 1000 Hz with an analogue filtering of 0.1–330 Hz. Prior to the measurements, we accommodated the sound volume at 50 dB above the minimum hearing threshold of each participant. Moreover, by utilizing a 3D digitizer (Polhemus Fastrak, Colchester, VT, USA), we registered the participant's head shape and the position of four headcoils, with respect to three anatomical landmarks (nasion, and left and right preauricular locations). This information was successively used to co-register the MEG data with the anatomical structure collected by the MRI scanner. The location of the headcoils was registered during the entire recording by using a continuous head position identification (cHPI), allowing us to track the exact head location within the MEG scanner at each time-point. We utilized this data to perform an accurate movement correction at a later stage of data analysis.

The recorded MRI data corresponded to structural T1. The acquisition parameters for the scan were: voxel size = 1.0 x 1.0 x 1.0 mm (or 1.0 mm^3); reconstructed matrix size 256×256; echo time (TE) of 2.96 ms and repetition time (TR) of 5000 ms and a bandwidth of 240 Hz/Px. Each individual T1-weighted MRI scan was successively co-registered to the standard Montreal Neurological Institute (MNI) brain template through an affine transformation and then referenced to the MEG sensors space by using the Polhemus head shape data and the three fiducial points measured during the MEG session.

Data pre-processing

The raw MEG sensor data (204 planar gradiometers and 102 magnetometers) was pre-processed by MaxFilter [50] for attenuating the interference originated outside the scalp by applying signal space separation. Within the same session, Maxfilter also adjusted the signal for head movement and down-sampled it from 1000 Hz to 250 Hz.

The data was converted into the Statistical Parametric Mapping (SPM) format and further analyzed in Matlab (MathWorks, Natick, Massachusetts, United States of America) by using Oxford Centre for Human Brain Activity Software Library (OSL) [51], a freely available toolbox that combines in-house-built functions with existing tools from the FMRIB Software Library (FSL) [52], SPM [53] and Fieldtrip [54]. The data was then high-pass filtered (0.1 Hz threshold) to remove frequencies that were too low for being originated by the brain. We also

applied notch filter (48-52 Hz) to correct for possible interference of the electric current. The data was further downsampled to 150 Hz and few parts of the data, altered by large artefacts, were removed after visual inspection. Then, to discard the interference of eyeblinks and heart-beat artefacts from the brain data, we performed independent component analysis (ICA) to decompose the original signal in independent components. Then, we isolated and discarded the components that picked up eyeblink and heart-beat activities, rebuilding the signal by using the remaining components [55]. The data was epoched in 80 trials (one for each musical excerpt) lasting 3500 ms each (100ms of pre-stimulus time), and low-pass filtered (40Hz threshold) to improve the subsequent analysis.

Then, correctly identified trials were analysed by employing two different methodologies (multivariate pattern analysis and cluster-based MCS of independent univariate analyses) to strengthen the reliability of the results as well as to increment the amount of information derived by the data.

Multivariate pattern analysis

We conducted a multivariate pattern analysis to decode different neural activity associated to the recognition of Bach's original patterns and variations. Specifically, we employed SVMs (libsvm:http://www.csie.ntu.edu.tw/~cjlin/libsvm/) [56], analysing each participant independently. MEG data was arranged in a 3D matrix (channels x time-points x trials) and submitted to the supervised learning algorithm. To avoid overfitting, we employed a leave-one-out cross-validation approach to train the SVM classifier to decode the two conditions. This procedure consisted of dividing the trials into N (here with $N = 8$) different groups and, for each time point, assigning $N - 1$ groups to the training set and the remaining N^{th} group to the testing set. Then, the performance of the classifier to separate the two conditions was evaluated. This process was carried out 100 times with random reassignment of the data to training and testing sets. Finally, the decoding accuracy time-series were averaged together to obtain a final time-series reflecting the performance of the classifier for each participant.

Then, to identify the channels that were carrying the highest amount of information required for decoding the two experimental conditions, we followed the procedure described by Haufe and colleagues [57] and computed the decoding patterns from the weights returned by the SVM.

Finally, to assess whether the two experimental conditions were differentiated by neural patterns stable over time, we performed a temporal generalization multivariate analysis. The algorithm was the same as the one described above, with the difference that in this case we

used each time-point of the training set to predict not only the same time-point in the testing set, but all time-points [58,59,60].

In both cases, to test whether the decoding results were significantly different from the chance level (50%), we used a sign permutation tests against the chance level for each time-point ($\alpha = .05$) and then corrected for multiple comparisons by applying FDR correction ($p < .026$ for non-temporal generalization results and $p < .005$ for temporal generalization results).

Univariate tests and Monte Carlo simulations

The multivariate pattern analysis is a powerful tool that requires relatively few pre-processing steps for returning an estimation of the different neural activity associated to two or more experimental conditions. However, this technique does not identify which condition was stronger than the other nor the polarity of the neural signal characterising the experimental conditions. To answer these questions and strengthen our results, we employed a different approach by calculating several univariate t-tests and then correcting for multiple comparisons by using MCS.

Before computing the t-tests, in accordance with a large number of other MEG and electroencephalography (EEG) task studies [61,62], we averaged the trials over conditions, obtaining two mean trials, one for Bach's original and one for the variation. Then, we combined each pair of planar gradiometers by mean root square. Afterwards, we computed a t-test for each combined planar gradiometer and each time-point in the time-range 0 – 2.500 seconds, contrasting the two experimental conditions. We reshaped the matrix for obtaining, for each time-point, a 2D approximation of the MEG channels layout that we binarized according to the *p*-values obtained from the previous t-tests (threshold = .01) and the sign of *t*-values. The resulting 3D matrix (*M*) was therefore composed by 0s when the t-test was not significant and 1s when it was. Then, to correct for multiple comparisons, we identified the clusters of 1s and assessed their significance by running MCS. Specifically, we made 1000 permutations of the elements of the original binary matrix *M*, identified the maximum cluster size of 1s and built the distribution of the 1000 maximum cluster sizes. Finally, we considered significant the original clusters that had a size bigger than the 99.9% maximum cluster sizes of the permuted data. Considering that magnetometers (differently from combined gradiometers) maintain the double polarity of the magnetic field, contrasting two experimental conditions presents potential technical ambiguities, admitting the theoretical possibility that two neighbouring clusters with opposite polarity and depicting different

strengths between conditions (e.g. cond1 > cond2 (positive polarity) in cluster one and cond2 > cond1 (negative polarity) in cluster two) may be identified as one unique large (positive) cluster. For these reasons, at first, we carried out the algorithm by contrasting Bach's original vs variation for combined planar gradiometers only. Then, on the basis of the significant clusters emerged, we used the same algorithm one more time for magnetometers only, within the significant time-range emerging from the first MCS (in this case: 0.547 – 1.180 seconds). This procedure allowed us to obtain more reliable and complete information about the different neural signal associated to Bach's original and variation for both gradiometers and magnetometers. The whole MCS procedure was performed for Bach's original vs variation and vice versa.

Source reconstruction

Beamforming

The brain activity collected on the scalp by MEG channels was reconstructed in source space using OSL [51] to apply an overlapping-spheres forward model and a beamformer approach as inverse method [63] (**Figure 1B** and **1C**). We used an 8-mm grid and both magnetometers and planar gradiometers. The spheres model depicted the MNI-co-registered anatomy as a simplified geometric model using a basic set of spherical harmonic volumes [64]. The beamforming utilized a diverse set of weights sequentially applied to the source locations for isolating the contribution of each source to the activity recorded by the MEG channels for each time-point [65,63].

General Linear Model

An independent GLM was calculated sequentially for each time-point at each dipole location, and for each experimental condition [66]. At first, reconstructed data was tested against its own baseline to calculate the statistics of neural sources of the two conditions Bach's original and Bach variation. Then, after computing the absolute value of the reconstructed time-series to avoid sign ambiguity of the neural signal, first-level analysis was conducted, calculating contrast of parameter estimates (Bach's original vs variation) for each dipole and each time-point. Those results were submitted to a second-level analysis, using one-sample t-tests with spatially smoothed variance obtained with a Gaussian kernel (full-width at half-maximum: 50 mm).

Then, to correct for multiple comparisons, a cluster-based permutation test [66] with 5000 permutations has been computed on second-level analysis results, taking into account the significant time-range emerged from the MEG sensors MCS significant gradiometer cluster. Therefore, we performed one permutation test on source space, using an α level of .05, corresponding to a cluster forming threshold of $t = 1.7$.

Brain activity underlying musical patterns development

Then, as depicted in **Figure 1D**, we performed an additional analysis considering the brain activity underlying the processing of each tone forming the musical sequences. To do that we computed a GLM for each time-point and source location and then corrected for multiple comparisons with a cluster-based permutation test, as described above [66]. Here, when computing the significant clusters of brain activation independently for the two experimental conditions (Bach's original and variation), we computed 10 permutation tests on source space, adjusting the α level to .005 (.05/10), corresponding to a cluster forming threshold of $t = 2.7$. Regarding Bach's original vs variation, we performed five tests and therefore the α level became .01 (.05/5), corresponding to a cluster forming threshold of $t = 2.3$.

Functional connectivity pre-processing

Regarding functional connectivity analysis, we used slightly larger epochs (pre-stimulus time of 200ms instead of 100ms). After reconstructing the data into source space, we constrained the beamforming results into the 90 non-cerebellar regions of the AAL parcellation, a widely-used and freely available template [67] in line with previous MEG studies [68,69,70] and corrected for source leakage [71]. Finally, according to a large number of MEG and EEG task studies [61,62] we averaged the trials over conditions, obtaining two mean trials, one for Bach's original and one for Bach variation. In order to minimize the probability of analyzing trials that were correctly recognised by chance, here we only considered the 20 fastest (mean RT: 1770 ± 352 ms) correctly recognised original (mean RT: 1717 ± 381 ms) and variation (mean RT: 1822 ± 323 ms) excerpts. The same operation has been carried out for the resting state that served as baseline. Here, we created 80 pseudo-trials with the same length of the real ones, starting at random time-points of the recorded resting state data.

This procedure has been carried out for five different frequency bands (delta: 0.1 – 2 Hz, theta: 2 – 8 Hz alpha: 8 – 12 Hz, beta: 12 – 32 Hz, gamma: 32 – 75 Hz) [72].

Static functional connectivity and degree centrality

We estimated the SFC calculating Pearson's correlations between the envelope of each pair of brain areas time-courses. This procedure has been carried out for both task and baseline and for each of the five frequency bands considered in the study. Afterwards, we averaged the connectivity matrices in order to obtain one global value of connectivity for each participant and each frequency band. These values were submitted to an ANOVA to highlight which frequency band yielded the clearest connectivity results, as illustrated in **Figure 5B** [73]. Successive post-hoc analysis was done by using Tukey's correction for multiple comparisons. Then, for all frequency bands, we computed Wilcoxon sign-rank tests comparing each pair of brain areas for recognition task vs baseline, aiming to identify the functional connectivity specifically associated to the task. To evaluate the outputted connectivity matrix *B*, we identified the degree of each region of interest (ROI) and tested its significance through MCS [74].

In graph theory the degree of each vertex *v* (here each brain area) of the graph *G* (here the matrix *B*) is given by the sum of the connection strengths of *v* with the other vertexes of *G*, showing the centrality of each *v* in *G* [75]. We computed the degree of each vertex of *B* for each musical tone, obtaining a 90 x 1 vector (s_t). Then, through MCS, we assessed whether the vertices of *B* had a significantly higher degree than the degrees obtained permuting *B*. Specifically, we made 1000 permutations of the elements in the upper triangle of *B* and we calculated a 90 x 1 vector $d_{v,p}$ containing the degree of each vertex *v* for each permutation *p*. Combining vectors $d_{v,p}$ we obtained the distribution of the degrees calculated for each permutation. Finally, we considered significant the original degrees stored in s_t that randomly occurred during the 1000 permutations less than two times. This threshold was obtained by dividing the α level (.001) by the five frequency bands considered in the study. The α level was set to .001 since this is the threshold that, during simulations with input matrices of uniformly distributed random numbers, provided no false positives. This procedure was carried out for each frequency band and for both experimental conditions.

Phase synchronization estimation

In order to reveal the brain dynamics of the musical sequence recognition, we studied the phase synchronization between brain areas for theta, the frequency band that showed the strongest connectivity patterns when contrasting task vs baseline at the previous stage of analysis.

As illustrated in **Figure 2A**, by applying the Hilbert transform [76] on the envelope of the reconstructed time-courses we obtained the analytic signal expressed by the following equation:

$$S_{(n_i,t)} = A_{(n_i,t)} e^{j\theta_{(n_i,t)}} \quad (3)$$

where $A_{(n_i,t)}$ refers to the instantaneous amplitude and $\theta_{(n_i,t)}$ to the instantaneous phase of the signal for the brain region n_i at time t. To prevent boundary artefacts due to the instantaneous phase estimation [77], we computed the Hilbert transform on time-series that were slightly larger than the duration of the stimuli and then discarded their edges. To estimate the phase synchronization between two brain areas n_i and n_m, after extracting the instantaneous phase at time t, we calculated the cosine similarity expressed by equation (4):

$$IFC_{(n_i,n_m,t)} = \cos(\theta_{(n_i,t)} - \theta_{(n_m,t)}) \quad (4)$$

We carried out this procedure for each time-point and each pair of brain areas, obtaining 90 x 90 symmetric IFC matrices showing the phase synchronization of every couple of brain areas over time. This calculation has been performed for the two conditions (Bach's original and variation) and for the baseline, as depicted in **Figure 2B**.

Dynamic functional connectivity and degree centrality

Since we were interested in detecting the brain connectivity profile and dynamics associated to the processing of each tone of the musical sequence, we sub-averaged the IFC matrices to obtain one sub-averaged IFC matrix for each tone and condition. This procedure allowed us to reduce data dimensionality and remove random noise introduced by the signal processing.

To detect the brain connectivity specifically associated to the task we applied Wilcoxon signed-rank tests, contrasting, for each pair of brain areas, each of the five sub-averaged IFC matrices of the task with the averaged values over time of the baseline, as depicted in **Figure 2C**. This procedure allowed us to obtain a square matrix for each tone (B_t) and for both

conditions (Bach's original and variation) showing the strength of the phase synchronisation between each pair of brain areas during the evolution of the task. After this procedure, we calculated an MCS (**Figure SF4**) analogous to the one described above for the SFC to test which ROIs were significantly central within the brain network for the recognition of Bach's original and variation. Since we repeated this test 10 times (two conditions and five tones), we used a threshold = 1.0e-04, obtained dividing the α level (.001) by 10. **Figure 2D** provides a graphical representation of the whole-brain connectivity and the correspondent degree centrality calculation. Finally, we contrasted the IFC matrices of Bach's original vs variation and vice versa and we submitted the results to MCS. In this case, since we computed five independent tests (Bach's original vs variation and Bach variation vs original), we obtained a threshold = 2.0e-04 (α level divided by five). We indicated the output of this calculation instantaneous brain degree ($IBD_{(t)}$).

Kuramoto order parameter

In conclusion, we computed the Kuramoto order parameter to estimate the global synchronization between brain areas over time. This parameter is defined by equation (5):

$$R_{(t)} = \left| \sum_{n=1}^{N} e^{i\theta_{(n,t)}} \right| / N \qquad (5)$$

where $\theta_{(n,t)}$ is the instantaneous phase of the signal for the brain region n at time t. The Kuramoto order parameter indicates the global level of synchronization of a group of N oscillating signals [78,79]. Thus, if the signals are completely independent the N instantaneous phases are uniformly distributed and therefore $R_{(t)}$ tends to 0. In contrast, if the N phases are equal, $R_{(t)}$ = 1.

The time-series obtained for Bach's original and variation were then contrasted by calculating t-tests and binarized, assigning 1 to significant values (threshold = .05) emerged from t-tests and 0 otherwise. Those values were submitted to a 1D MCS. For each of the 10000 permutations, we randomized the binarized elements (threshold = .05) of the *p*-value time-series and extracted the maximum cluster size. Then, we built a distribution of

maximum cluster sizes and considered significant the original clusters that were larger than the 95% of the permuted ones.

Acknowledgements

We thank Giulia Donati, Riccardo Proietti, Giulio Carraturo, Mick Holt and Holger Friis for their assistance in the neuroscientific experiment. We also thank the psychologist Tina Birgitte Wisbech Carstensen for her help with the administration of psychological tests and questionnaires.

The Center for Music in the Brain (MIB) is funded by the Danish National Research Foundation (project number DNRF117). Additionally, we thank the Italian section *of Mensa: The International High IQ Society* for the economic support provided to the author Francesco Carlomagno and the University of Bologna for the economic support provided to the students Giulia Donati, Riccardo Proietti, Giulio Carraturo.

MLK is supported by the ERC Consolidator Grant: CAREGIVING (n. 615539), Center for Music in the Brain, funded by the Danish National Research Foundation (DNRF117), and Centre for Eudaimonia and Human Flourishing funded by the Pettit and Carlsberg Foundations.

GD is supported by the Spanish Research Project PSI2016-75688-P (AEI/FEDER, EU), by the European Union's Horizon 2020 Research and Innovation Programme under grant agreements n. 720270 (HBP SGA1) and n. 785907 (HBP SGA2), and by the Catalan AGAUR Programme 2017 SGR 1545.

JC is supported by Portuguese Foundation for Science and Technology CEECIND/03325/2017, Portugal.

Author contributions

LB, EB, MLK and PV conceived the hypotheses and designed the study. LB, FC, JC, AS, DP, MLK performed pre-processing and statistical analysis. GD, MP, EB, MLK, DP, PCW and PV provided essential help to interpret and frame the results within the neuroscientific literature. LB wrote the first draft of the manuscript and, together with FC and MLK, prepared the figures. All the authors contributed to and approved the final version of the manuscript.

Competing interests statement

The authors declare no competing interests.

References

[1] Friston, K., & Kiebel, S. Predictive coding under the free-energy principle. *Philosophical Transactions of the Royal Society B: Biological Sciences*, 364(1521), 1211-1221 (2009).

[2] Koelsch, S., Vuust, P., & Friston, K. Predictive Processes and the Peculiar Case of Music. Trends in Cognitive Sciences, 23(1), 63-77 (2019).

[3] Dehaene, S., Kerszberg, M., & Changeux, J. P. A neuronal model of a global workspace in effortful cognitive tasks. *Proceedings of the National Academy of Sciences of the United States of America*, **95(24)**, 14529-14534 (1998).

[4] Patel, A. D. *Music, Language, and the Brain* (Oxford University Press, Oxford, 2008).

[5] Wixted, J. T. Dual-process theory and signal-detection theory of recognition memory. *Psychological Review* **114(1)**, 152-176 (2007).

[6] Yonelinas, A. P. The nature of recollection and familiarity: A review of 30 years of research. *Journal of Memory and Language* **46(3)**, 441-517 (2002).

[7] Eichenbaum, H., Yonelinas, A. P., & Ranganath, C. The Medial Temporal Lobe and Recognition Memory. *Annual Review of Neuroscience*, 30, 123-152 (2007).

[8] Aggleton, J. P., & Brown, M. W. Interleaving brain systems for episodic and recognition memory. *Trends in Cognitive Sciences,* **10(10)**, 455-643. (2006).

[9] DiCarlo, J. J., Zoccolan, D., & Rust, N. C. How does the brain solve visual object recognition? *Neuron*, 73(3), 415-34 (2012).

[10] Brattico, E., Näätänen, R., & Tervaniemi, M. Context effects on pitch perception in musicians and nonmusicians: Evidence from event-related potential recordings. *Music Perception*, **19(2)**, 199–222 (2001).

[11] Näätänen, R., Paavilainen, P., Rinne, T., & Alho, K. The mismatch negativity (MMN) in basic research of central auditory processing: A review. *Clinical Neurophysiology* **118(12)**, 2544-2590 (2007).

[12] Dehaene, S., Meyniel, F., Wacongne, C., Wang, L., & Pallier, C. The Neural Representation of Sequences: From Transition Probabilities to Algebraic Patterns and Linguistic Trees. *Neuron*, **88(1)**, 2-19 (2015).

[13] Peretz, I., & Zatorre, R. J. *The Cognitive Neuroscience of Music* (Oxford University Press, Oxford, 2003).

[14] Raynor, H., & Cooke, D. *The Language of Music* (Oxford University Press, Oxford, 1960).

[15] Plack, C. J. *The sense of hearing* (Lawrence Erlbaum Associates Publishers, Mahwah, 2005).

[16] Williams, P. J. S. *Bach: A Life in Music* (Cambridge University Press, Cambridge, 2007).

[17] Hofstadter, D. R. Gödel, Escher, Bach: An Eternal Golden Braid (Basic Books, New York, 1999).

[18] Changeux, J. P. *Secrets of Creativity: What Neuroscience, the Arts, and Our Minds Reveal*. (Oxford University Press, Oxford, 2019).

[19] Stark, E. A., Vuust, P., & Kringelbach, M. L. Music, dance, and other art forms: New insights into the links between hedonia (pleasure) and eudaimonia (well-being). *Progress in Brain Research* **237**, 129-152 (2018).

[20] Näätänen, R., Pakarinen, S., Rinne, T., & Takegata, R. The mismatch negativity (MMN): Towards the optimal paradigm. *Clinical Neurophysiology* **115(1)**, 140-144 (2004).

[21] Remedios, R., Logothetis, N. K., & Kayser, C. An auditory region in the primate insular cortex responding preferentially to vocal communication sounds. *Journal of Neuroscience* **29(4)**, 1034-1045 (2009).

[22] Bird, C. M. The role of the hippocampus in recognition memory. Cortex **93**, 155-165 (2017).

[23] Brown, M. W., & Aggleton, J. P. Recognition memory: What are the roles of the perirhinal cortex and hippocampus? *Nature Reviews Neuroscience,* **2(1)**, 51-61 (2001).

[24] Teixeira, C. M., Pomedli, S. R., Maei, H. R., Kee, N., & Frankland, P. W. Involvement of the anterior cingulate cortex in the expression of remote spatial memory. *Journal of Neuroscience* **26(29)**, 7555-7564 (2006).

[25] Bach, D. R. et al. The effect of appraisal level on processing of emotional prosody in meaningless speech. *NeuroImage,* **42(2)**, 919-927 (2008).

[26] Stephenson-Jones et al. A basal ganglia circuit for evaluating action outcomes. *Nature* **539(7628)**, 289-293 (2016).

[27] Kringelbach, M. L. The hedonic brain: a functional neuroanatomy of human pleasure. *Pleasures of the Brain*, 13(11), 479-487 (2009).

[28] Vuust, P., & Kringelbach, M. L. The pleasure of making sense of music. *Interdisciplinary Science Reviews* **35(2)**, 166-182 (2010).

[29] Zatorre, R. J., Belin, P., & Penhune, V. B. Structure and function of auditory cortex: Music and speech. *Trends in Cognitive Sciences* **6(1)**, 37-46 (2002).

[30] Limongi, R., Sutherland, S. C., Zhu, J., Young, M. E., & Habib, R. Temporal prediction errors modulate cingulate-insular coupling. *NeuroImage*, 71, 147-157 (2013).

[31] Koelsch, S., Fritz, T., Cramon, D. Y. V., Müller, K., & Friederici, A. D. Investigating emotion with music: An fMRI study. *Human Brain Mapping*, 27(3), 239-250 (2006).

[32] Stephenson-Jones, M., Kardamakis, A. A., Robertson, B., & Grillner, S. Independent circuits in the basal ganglia for the evaluation and selection of actions. *Proceedings of the National Academy of Sciences of the United States of America* **110(38)**, 3670-3679 (2013).

[33] Squire, L. R., & Bayley, P. J. The neuroscience of remote memory. *Current Opinion in Neurobiology* **17(2)**, 185-196 (2007).

[34] Packard, M. G., & Knowlton, B. J. Learning and Memory Functions of the Basal Ganglia. *Annual Review of Neuroscience* **25**, 563-593 (2002).

[35] Dehaene, S., & Changeux, J. P. Experimental and Theoretical Approaches to Conscious Processing. *Neuron*, **70(2)**, 200-227 (2011).

[36] Dehaene, S., Changeux, J. P., & Naccache, L. The global neuronal workspace model of conscious access: From neuronal architectures to clinical applications. *Research and Perspectives in Neurosciences*, 55-84 (2011).

[37] Dehaene, S., & Changeux, J. P. Ongoing spontaneous activity controls access to consciousness: A neuronal model for inattentional blindness. *PLoS Biology*, **3(5)**, e141 (2005).

[38] Brown, J. W., & Braver, T. S. Learned predictions of error likelihood in the anterior cingulate cortex. *Science,* **307(5712)**, 1118-1121 (2005).

[39] Holroyd, C. B. et al. Dorsal anterior cingulate cortex shows fMRI response to internal and external error signals. *Nature Neuroscience*, 7(5), 497-498 (2004).

[40] Mack, M. L., Love, B. C., & Preston, A. R. Building concepts one episode at a time: The hippocampus and concept formation. *Neuroscience Letters* **680**, 31-38 (2018).

[41] Shohamy, D., & Wagner, A. D. Integrating Memories in the Human Brain: Hippocampal-Midbrain Encoding of Overlapping Events. *Neuron* **60(2)**, 378-389 (2008).

[42] Näätänen, R., & Picton, T. The N1 Wave of the Human Electric and Magnetic Response to Sound: A Review and an Analysis of the Component Structure. *Psychophysiology* **24(4)**, 375-425 (1987).

[43] Parras, G. et al. Neurons along the auditory pathway exhibit a hierarchical organization of prediction error. *Nature Communications* **8(1)**, 1-17(2017).

[44] Wacongne, C. et al. Evidence for a hierarchy of predictions and prediction errors in human cortex. *Proceedings of the National Academy of Sciences of the United States of America* **108 (51)**, 20754-20759 (2011).

[45] Näätänen, R., Tervaniemi, M., Sussman, E., Paavilainen, P., & Winkler, I. "Primitive intelligence" in the auditory cortex. *Trends in Neurosciences* **24(5)**, 283-288 (2001).

[46] Walter, W. G., Cooper, R., Aldridge, V. J., McCallum, W. C., & Winter, A. L. Contingent negative variation: An electric sign of sensori-motor association and expectancy in the human brain. *Nature* **203**, 380-384 (1964).

[47] Kayser, J., Fong, R., Tenke, C. E., & Bruder, G. E. Event-related brain potentials during auditory and visual word recognition memory tasks. *Cognitive Brain Research*, 16(1), 11-25 (2003).

References (Methods only)

[48] Pearce, M. T. Statistical learning and probabilistic prediction in music cognition: Mechanisms of stylistic enculturation. *Annals of the New York Academy of Sciences* **1423**(1), (2018).

[49] Sears, D. R. W., Pearce, M. T., Caplin, W.E & McAdams, S. Simulating melodic and harmonic expectations for tonal cadences using probabilistic models. *Journal of New Music Research* **47**, 29-52 (2018).

[50] Taulu, S. & Simola, J. Spatiotemporal signal space separation method for rejecting nearby interference in MEG measurements. *Physics in Medicine and Biology* **51**, 1759–1768 (2006).

[51] Woolrich, M. W., Hunt, L., Groves, A., Barnes, G. MEG beamforming using Bayesian PCA for adaptive data covariance matrix regularization. *Neuroimage* **57(4)**, 1466-1479 (2011).

[52] Woolrich, M. W. et al. Bayesian analysis of neuroimaging data in FSL. *NeuroImage* **45**, S173-S186 (2009).

[53] Penny, W., Friston, K., Ashburner, J., Kiebel, S., & Nichols, T. *Statistical Parametric Mapping: The Analysis of Functional Brain Images. Statistical Parametric Mapping: The Analysis of Functional Brain Images*. (Academic Press, Cambridge, USA, 2007).

[54] Oostenveld, R., Fries, P., Maris, E., Schoffelen, J. M. FieldTrip: Open source software for advanced analysis of MEG, EEG, and invasive electrophysiological data. *Computational Intelligence and Neuroscience* **2011**, 156869 (2011).

[55] Mantini, D. et al. A signal-processing pipeline for magnetoencephalography resting-state networks. *Brain Connectivity* **1(1)**, 49-59 (2011).

[56] Wilson, M. D. *Support Vector Machines*. In Encyclopedia of Ecology, Five-Volume Set, (Academic Press, Cambridge, USA, 3431-3437, 2008).

[57] Haufe, S. et al. On the Interpretation of Weight Vectors of Linear Models in Multivariate. *Neuroimaging* **87**, 96-110 (2014).

[58] Cichy, R. M., Pantazis, D., & Oliva, A. Resolving human object recognition in space and time. Nature Neuroscience, **17(3)**, 455-462 (2014).

[59] King, J. R., & Dehaene, S. Characterizing the dynamics of mental representations: The temporal generalization method. *Trends in Cognitive Sciences*, 18(4), 203-210 (2014).

[60] Pantazis, D. et al. Decoding the orientation of contrast edges from MEG evoked and induced responses. *NeuroImage* **180**, 267-279 (2018).

[61] Gross, J. et al. Good practice for conducting and reporting MEG research. *NeuroImage* **65**, 349-363 (2013).

[62] Keil, A. et al. Committee report: Publication guidelines and recommendations for studies using electroencephalography and magnetoencephalography. *Psychophysiology* **51**, 1–21 (2014).

[63] Hillebrand, A. & Barnes, G. R. Beamformer analysis of MEG data. *International Review of Neurobiology* **68**, 149-171 (2005).

[64] Huang, M. X., Mosher, J. C. & Leahy, R. M. A sensor-weighted overlapping-sphere head model and exhaustive head model comparison for MEG. *Physics in Medicine and Biology* **44**, 423-440 (1999).

[65] Brookes, M. J. et al. Beamformer reconstruction of correlated sources using a modified source model. *NeuroImage* **34**, 1454–1465 (2007).

[66] Hunt, L. T. et al. Mechanisms underlying cortical activity during value-guided choice. *Nature Neuroscience* **15**, 470–476 (2012).

[67] Tzourio-Mazoyer, N. et al. Automated anatomical labeling of activations in SPM using a macroscopic anatomical parcellation of the MNI MRI-single-subject brain. *NeuroImage* **15**, 273–289 (2002).

[68] Brookes, M. J. et al. A multi-layer network approach to MEG connectivity analysis. *NeuroImage* **132**, 425–438 (2016).

[69] Cabral, J. et al. Exploring mechanisms of spontaneous functional connectivity in MEG: how delayed network interactions lead to structured amplitude envelopes of band-pass filtered oscillations. *NeuroImage* **90**, 423–435 (2014).

[70] Hindriks, R. et al. Role of white-matter pathways in coordinating alpha oscillations in resting visual cortex. *NeuroImage* **106**, 328–339 (2015).

[71] Colclough, G. L., Brookes, M. J., Smith, S. M. & Woolrich, M.W. A symmetric multivariate leakage correction for MEG connectomes. *NeuroImage* **117**, 439–448 (2015).

[72] Lee, D. J., Kulubya, E., Goldin, P., Goodarzi, A., & Girgis, F. Review of the neural oscillations underlying meditation. *Frontiers in Neuroscience* **12**, 178 (2018).

[73] Allen, M., Poggiali, D., Whitaker, K., Marshall, T. R., Kievit, A. R. Raincloud Plots: A Multi-Platform Tool for Robust Data Visualization. *Wellcome Open Research* **1**, 4:63 (2019).

[74] Kroese, D. P., Taimre, T., & Botev, Z. I. *Handbook of Monte Carlo Methods. Handbook of Monte Carlo Methods* (John Wiley and Sons, New York, 2011).

[75] Rubinov, M. & Sporns, O. Complex network measures of brain connectivity: Uses and Interpretations. *NeuroImage* **52**, 1059-1069 (2010).

[76] Layer, E., & Tomczyk, K. Hilbert transform. *Studies in Systems, Decision and Control* **16**, 107-116 (2015).

[77] Cabral, J. et al. Cognitive performance in healthy older adults relates to spontaneous switching between states of functional connectivity during rest. *Scientific Reports* **7**, 5135 (2017).

[78] Witthaut, D., & Timme, M. Kuramoto dynamics in Hamiltonian systems. *Physical Review E - Statistical, Nonlinear, and Soft Matter Physics* **90**(3), (2014).

[79] Kuramoto, Y. *Chemical Oscillations, Waves, and Turbulence* (Springer-Verlag, New York, 1984).